Investigation of Potential-Induced Degradation in Perovskite Solar Cells under Inert Conditions

BREUGELMANS, Robbe; LAMMAR, Stijn; AGUIRRE, Aranzazu; AERNOUTS, Tom; VERMANG, Bart & DAENEN, Michael (2025) Investigation of Potential-Induced Degradation in Perovskite Solar Cells under Inert Conditions. In: Solar RRL, 9 (7) (Art N° e2400923).

DOI: 10.1002/solr.202400923
Handle: http://hdl.handle.net/1942/45748

Investigation of Potential-Induced Degradation in Perovskite Solar Cells under Inert Conditions

*Robbe Breugelmans Stijn Lammar Aranzazu Aguirre Tom Aernouts Bart Vermang Michaël Daenen **

Ing. R. Breugelmans, Dr. Ir. S. Lammar, Dr. A. Aguirre, Dr. T. Aernouts, Prof. Dr. B. Vermang, Prof. Dr. Ir. M. Daenen
Hasselt University, imo-imomec, Martelarenlaan 42, 3500 Hasselt, Belgium

Ing. R. Breugelmans, Dr. Ir. S. Lammar, Dr. A. Aguirre, Dr. T. Aernouts, Prof. Dr. B. Vermang, Prof. Dr. Ir. M. Daenen
Imec, imo-imomec, Thor Park 8320, 3600 Genk, Belgium

Ing. R. Breugelmans, Dr. Ir. S. Lammar, Dr. A. Aguirre, Dr. T. Aernouts, Prof. Dr. B. Vermang, Prof. Dr. Ir. M. Daenen
EnergyVille, imo-imomec, Thor Park 8320, 3600 Genk, Belgium

Dr. Ir. S. Lammar
Department of Electrical Engineering (ESAT), KU Leuven, Kasteelpark Arenberg 10, 3001 Leuven, Belgium

Email Address: Michael.Daenen@uhasselt.be

Keywords: *Potential-induced degradation, Sodium ions, XRD, ToF-SIMS, PL*

Perovskite solar cells (PSCs) have emerged as a promising photovoltaic technology due to their remarkable efficiency advancements. However, their commercialization is hindered by stability challenges, including sensitivity to environmental conditions and a critical degradation mechanism known as potential-induced degradation (PID). PID can significantly impair PSC performance within hours under operational conditions. This study investigates PID in 48 triple-cation p-i-n PSCs over 313 hours in an inert environment, excluding additional stressors like moisture and oxygen. The PID-stressed devices degraded to 79% of their initial efficiency, primarily driven by losses in short-circuit current density. Time-of-flight secondary ion mass spectroscopy revealed sodium ion migration from soda-lime glass substrates into the perovskite layer. Interestingly, photoluminescence and X-ray diffraction analyses detected no measurable differences between PID-stressed and reference devices, contradicting prior literature that associates PID with perovskite segregation and decomposition. These findings challenge the conventional understanding of PID, suggesting that environmental factors such as oxygen and moisture might exacerbate degradation effects. This work provides critical insights into the intrinsic mechanisms of PID under controlled conditions and highlights the need for further research into the interplay between PID and environmental stressors to guide the development of more stable PSC technologies.

1 Introduction

Solar energy technology has evolved significantly over the years, with thin-film perovskite photovoltaic (PV) technology emerging as a highly promising advancement in solar energy, offering substantial potential for high-efficiency, low-cost, and versatile applications that extend beyond the limitations of traditional silicon-based PV [1,2]. Perovskite materials exhibit exceptional optoelectronic properties, such as micrometer-scale diffusion lengths surpassing their sub-micrometer thickness together with direct and tunable bandgaps, rendering them ideal candidates for PV applications and tandem integration with other PV technologies [1–5]. Despite being the fastest-evolving PV technology in terms of cell efficiency, the commercial deployment of perovskite solar cells is hindered by their low reliability, which compromises their long-term performance [6–8].

Perovskite solar cells (PSCs) are known to be highly sensitive to ambient conditions, including exposure to moisture, oxygen, light, and elevated temperatures [2, 4, 8–11]. It is possible to protect PSCs from moisture and oxygen exposure by effectively encapsulating the devices using UV-curable adhesive encapsulation or glass-glass vacuum lamination with polymers such as ethylene vinyl acetate (EVA), polyolefin (POE) or thermoplastic polyolefin (TPO) [12]. For laboratory-scale devices, encapsulation using epoxy resins is frequently employed, which can release volatile gases that can react with the perovskite [13].

In practical applications, PV modules are connected in series, leading to voltage accumulation. With the use of cost-effective transformer-less inverters, these systems often experience significant positive or negative voltage buildup. The PV frames are always grounded for safety reasons, resulting in potential differences between the frame and the PV cells, which can lead to a degradation phenomenon known as potential-induced degradation (PID) [14]. While PID has been extensively studied in silicon-based PV systems, its impact on perovskite devices is still in the early stages of investigation. Addressing this issue is critical to ensure the long-term stability and commercial viability of perovskite solar technologies [15].

Only a limited number of studies have investigated PID in PSCs [16–24]. In most cases, almost complete degradation was observed within less than 96 hours [16, 18–22]. Furthermore, Nakka et al. [18], demonstrated that the impact of PID stress was significantly amplified under elevated environmental conditions i.e., 25°C, 20% relative humidity (RH), to 60°C, 60% RH. This rapid deterioration of performance highlights PID as an aggressive degradation mechanism. Hence, it is crucial to gain a deeper understanding of this phenomenon in order to design effective mitigation or prevention strategies. Previous investigations have identified the migration of sodium ions (Na^+) from the soda-lime glass (SLG) substrate toward the device as the primary cause of PID [17, 18, 22]. These ions drift under the influence of an electric field toward the indium tin oxide (ITO) front contact, eventually diffusing throughout the PSC [17, 18, 22].

3D time-of-flight secondary ion mass spectroscopy (ToF-SIMS) showed that sodium shunt paths are formed through the device [17, 22]. Moreover, it has been proposed that Na^+ migration contributes to perovskite degradation by inducing segregation and decomposition, as evidenced by alterations in photoluminescence (PL) [18, 19, 21, 22] and X-ray diffraction (XRD) measurements [18, 19], potentially resulting in the formation of sodium-iodide (NaI) [18]. Interestingly, reversing the PID stress from -1000 V to +1000 V has shown partial recovery in PSC performance, offering critical insights for developing recovery strategies [16–18, 23]. The decrease in efficiency is primarily attributed to a reduction in short-circuit current density (J_{SC}), modifications in the fill factor (FF), and minimal losses in open-circuit voltage (V_{OC}) [16, 18, 19, 23, 24]. Nakka et al. proposed a first mitigation strategy by incorporating a nickel oxide (NiO_X) layer between the ITO front contact and the self-assembled monolayer (SAM), which significantly reduced PID effects [19].

Most PID studies have been conducted on encapsulated devices using epoxy resin under ambient conditions [17–19, 21]. However, device encapsulation must be carefully executed using appropriate materials that do not chemically interact with the perovskite and effectively prevent moisture and oxygen ingress [13].

In a previous work [23], we acknowledged the challenges associated with effective encapsulation and proposed a novel method for conducting PID stress tests in a nitrogen (N_2) environment. This approach eliminated the need for encapsulation by excluding moisture and oxygen in an inert environment, thus aiming to focus solely on the PID mechanism. As a result, a slower degradation rate was observed [23]. Afterward, in parallel, a similar approach was presented by Zhang et al. [22]. While this method is conceptually straightforward, achieving complete exclusion of external stressors remains challenging and requires dedicated equipment.

Considering the inherent susceptibility of PSCs to ambient conditions and their potential impact during PID stress tests [18], we believe that eliminating as many potential stressors as possible (i.e., moisture, oxygen, temperature, encapsulation) may result in degradation mechanisms that deviate from those previously reported in the literature. This study aims to provide novel insights by conducting PID stress tests on non-encapsulated triple-cation (3C) p-i-n PSCs in an inert environment. Furthermore, this work employs a range of characterization techniques, including microstructural analysis, to validate or challenge previous findings.

2 Methods and materials

This study explores the susceptibility of 3C p-i-n PSCs to PID. The perovskite composition is $Cs_{0.05}FA_{0.85}MA_{0.10}PbI_{2.90}Br_{0.10}$. The experiment spanned a total duration of 313 hours and involved six SLG substrates, each comprising 12 PSCs with an identical layer stack and an active area of 0.125 cm^2. The devices

were divided into two groups: a PID-stressed group and a control group. This distribution resulted in 48 PID-stressed PSCs and 24 control PSCs, the latter stored on a shelf under identical conditions but without exposure to PID stress. All devices were subjected to identical environmental conditions throughout the experiment, with the only variable being the PID stress.

Each device was constructed on 3 x 3 cm^2 SLG substrates with a 150 nm layer of ITO coating. A 15 nm NiO_X hole transport layer (HTL) was deposited via direct current (DC) sputtering from a metallic nickel target in oxygen plasma at 3 mTorr and annealed for 20 minutes in air at 300°C with relative humidity (RH) of 40-50%.

(4-(3,6-Dimethyl-9H-carbazol-9-yl)butyl)phosphonic acid (Me-4PACz) (1 mM in anhydrous ethanol) was used as a SAM. For the 3C perovskite devices, this SAM was sonicated at 30°C for 10 minutes before use. Then, it was spin-coated onto the glass/ITO at a speed of 3000 rpm for 30 s, followed by annealing at 100°C for 10 minutes. 1.3 M of the 3C perovskite was prepared by mixing 635.5 mg PbI_2, 197.3 mg FAI, 15.1 mg MABr, and 17.5 mg CsI in 1 ml of dimethylformamide (DMF) and N-methylpyrrolidon (NMP) (volume ratio = 9:1). The solution was stirred at room temperature for two days before use. A few hours prior to coating, 18 mol% of methylammonium chloride (MACl) was added to the precursor solution. The solution was dynamically spin-coated by a continuous two-step program: 2000 rpm for 10 s, followed by 6000 rpm for 45 s. During the second step, the perovskite film was quenched with N_2 for 30 s, starting at 40 s prior to the end of the spin coating program. This was followed by annealing the films at 130°C for 80 min in N_2.

Afterward, the electron transport layer (ETL) was evaporated, composed of 0.8 nm lithium fluoride (LiF), 60 nm C60, and a 5 nm bathocuproine (BCP) bilayer. Finally, a 100 nm copper (Cu) top electrode was evaporated to complete the devices.

During the PID stress, the devices were short-circuited to eliminate any external electric field across the device stack. PID occurs when PV devices are maintained at a high negative potential relative to the glass; thus, the short-circuited devices were subjected to -1000 V while a grounded Cu block was applied to the external surface of the SLG, as illustrated in Figure 1.

Perovskite devices are highly sensitive to ambient conditions, such as moisture, oxygen, and potential byproducts from encapsulation materials. Consequently, the entire experiment was performed in a N_2 environment on non-encapsulated devices, following recommendations from our previous study [23].

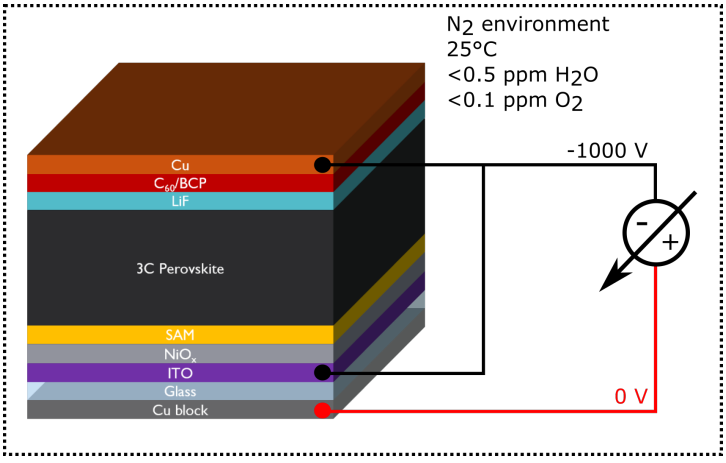

Figure 1: Schematical representation of the PID stress test in a N_2 environment. The contacts of the device are short-circuited and connected to a high negative potential of -1000 V, while 0 V is connected to a Cu block, which is pressed onto the external surface of the glass.

During the experiment, current-voltage (IV) measurements were performed at intermediate intervals in a N_2 environment using a Keithley 2620 A source-measure unit and an Abet solar simulator, providing one-sun illumination (1000 W/m^2, air mass (AM) 1.5 G). Prior to the measurements, a calibration was performed using a Fraunhofer ISE WPVS reference solar cell. IV sweeps were conducted from -0.2 V to 1.3 V in 0.01 V steps with a scanning speed of 0.8 V/s, and the temperature of the PSC device was controlled at 30°C using a fan.

External quantum efficiency (EQE) measurements were conducted in a N_2-filled holder at the start, and conclusion of the PID stress tests. A Bentham PVE300 spectral response setup equipped with halogen and xenon lamps was employed for the measurements. The tool was calibrated using a silicon (Si) reference cell to ensure accuracy. EQE spectra were recorded across a wavelength range of 300 to 900 nm with a step size of 5 nm, focusing on an area of 0.7 mm^2.

PL measurements were used to assess the optoelectronic properties of the stressed devices, with steady-state measurements covering a wavelength range from 730 to 850 nm in steps of 1 nm, using an integration time of 1 second. The measurements were performed in air using a PicoQuant FluoTime 300 instrument equipped with an LDH-P-C 440 laser source operating at 20 MHz. Furthermore, ToF-SIMS was conducted on one reference and one PID stressed PSC to investigate the migration of sodium ions from the SLG towards the device. Here, the positively charged ions were analyzed using the bombardment of cesium ions (Cs^+) and more information can be found in the supporting information.

Finally, XRD was performed to gain deeper insights into the effects of Na^+ migration on the crystallinity and degradation of the perovskite. The XRD measurements were performed in air by using a Bruker D8 diffractometer equipped with Cu-Kα X-rays (λ = 1,5418 Å). A measurement range was employed from 10° to 60° . Before conducting the XRD measurements, the Cu layer needed to be removed to expose the perovskite absorber layer. A peel-off method was conducted using tape to carefully remove the Cu layer from the PSC, ensuring proper access to the perovskite for accurate XRD analysis.

3 Results

Throughout the experiment, several intermediate IV measurements were performed to investigate the effects of Na^+ migration into the PSC. From these measurements, current density-voltage (JV) curves were derived. These measurements provide critical insights into the role of Na^+ migration in the degradation of PSC performance.

Figure 2 presents the normalized power conversion efficiency (PCE) as a function of stress duration for 48 stressed devices in red. Additionally, the graph shows the data for 24 PSCs, represented in grey, which were stored on the shelf under identical environmental conditions (i.e., N_2 atmosphere, ambient temperature) without without exposure to voltage stress, serving as control samples for the entire duration of the experiment.

By the end of the experiment, the PID-stressed PSCs reached an average normalized efficiency of 79%, while the control devices retained an average of 99% of their initial PCE. Notably, after only 154 hours, the PCE of the PID stressed devices had already declined to an average of 86%, highlighting that the most substantial PID-related degradation occurred within the first half of the testing period.

In order to gain insights into the mechanism of the degradation, the JV parameters were analyzed. The average normalized values for J_{SC}, V_{OC}, and FF were found to be 0.88, 0.98, and 0.91, respectively. These results indicate that the 48 PSCs primarily experienced losses in J_{SC}, moderate losses in FF, and minimal changes in V_{OC}, corroborating findings from our previous work [23].

A closer examination of the JV curve is essential for gaining deeper insights into the degradation mechanism. Hence, Figure 3 presents the JV curves of a PID-stressed device in both its initial and stressed states, accompanied by the EQE response shown in Figures (a) and (b), respectively.

The graphs in Figure 3 (a) clearly illustrate that the degradation was mainly driven by a drop in J_{SC}, modest changes in FF, but almost negligible changes in V_{OC}. Furthermore, from the JV graph, it can be observed that the drop in FF is attributed to an affected horizontal slope around J_{SC}, combined with changes in the vertical slope around V_{OC}. These observations suggest that PID stress may have contributed to a decrease in shunt resistance and an increase in series resistance within the device.

Additionally, EQE measurements were performed, as illustrated in Figure 3 (b), with results captured at the beginning and end of the PID stress test, shown in grey and red, respectively. It is noteworthy that the decrease in EQE in both graphs is not limited to a specific wavelength but instead shows a uniform vertical downward shift across the spectrum. This pattern indicates a general reduction in charge extraction efficiency, aligning with the observed reduction in J_{SC}.

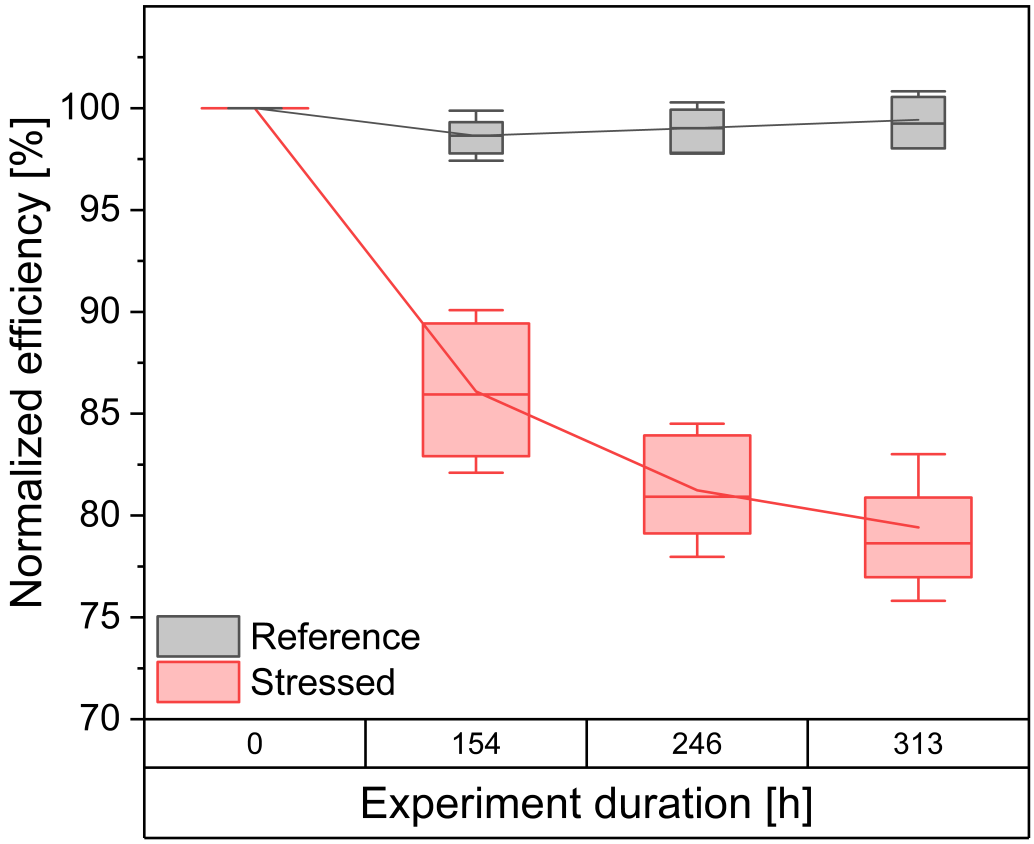

Figure 2: Normalized efficiency for the stressed 3C p-i-n PScs and reference devices as a control group, in red and grey, respectively. The height of the box charts indicates the interquartile range between 25% and 75% of the data. The whiskers show one standard deviation.

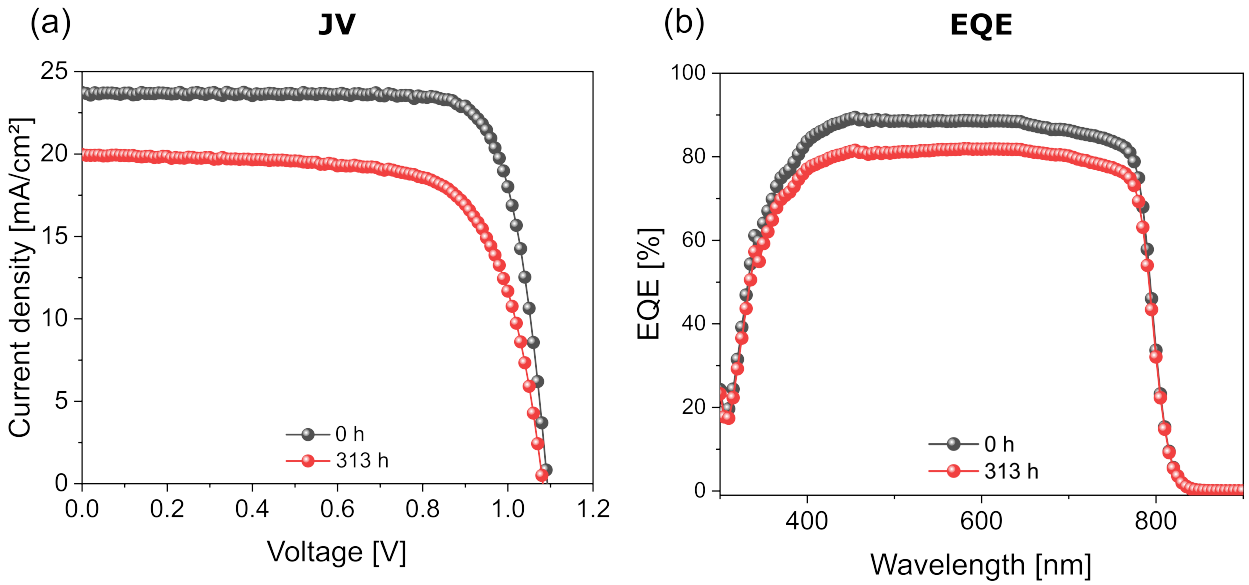

Figure 3: JV graphs (a) and EQE response (b) at the beginning and the end of the PID stress test in grey and red, respectively.

In addition to intermediate characterization methods, further analyses were conducted after the PID stress test. Accordingly, PL measurements were performed to assess potential changes in the bandgap

energy of the absorber material, attributed to chemical alterations such as perovskite segregation, as indicated by shifts in the peak intensity. Figure 4 shows the normalized intensities for a PID-stressed PSC and a reference one. It is to be noted that the PL device was not calibrated using a dedicated reference device prior to the measurements. Hence, changes in the absolute value of the PL response are not reliable. Since the main purpose of the measurement is the investigation of shifts in the PL peak intensity, the results have been normalized. The measurement revealed no significant shift in the peak emission wavelength between the stressed and reference, confirming that the peak position remained consistent between stressed and reference samples. Additionally, the minor variation in peak width was deemed negligible.

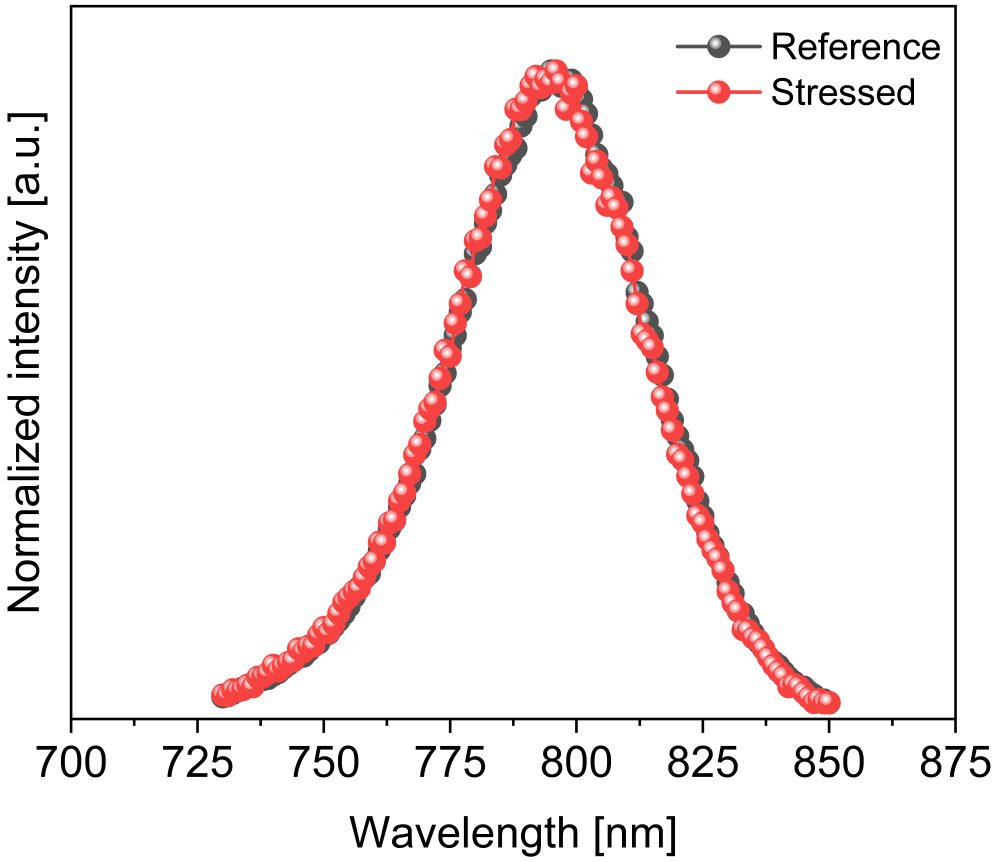

Figure 4: Normalized PL measurements of a reference and PID stressed PSC in grey and red, respectively.

Furthermore, microstructural analyses were conducted, including XRD measurements, to assess potential phase segregation induced by PID stress. Diffractograms were recorded in the 2θ-range 10° to 60° as shown in Figure 5, which depicts the XRD spectra for both the reference and stressed 3C devices. The reference data is shown in grey, while the stressed data is depicted in red, with a vertical offset applied for clarity. Notably, there is no observable difference between the XRD patterns for both, even around the diffraction from the PbI_2 at 12.5° marked by an asterisk. These results indicate that no substantial phase segregation or crystallographic changes occurred in the perovskite during the PID stress test.

To further investigate the role of Na^+ migration as the root cause of PID, ToF-SIMS measurements were conducted. Figure 6 presents the ToF-SIMS results for both reference and PID-stressed 3C PSCs. The graph presents the intensity as a function of the fluence, which correlates with scan time. It is important to note that the ToF-SIMS intensities have been rescaled for visualization purposes, and consequently, the absolute values of the measured elements should not be considered definitive. Given that the primary

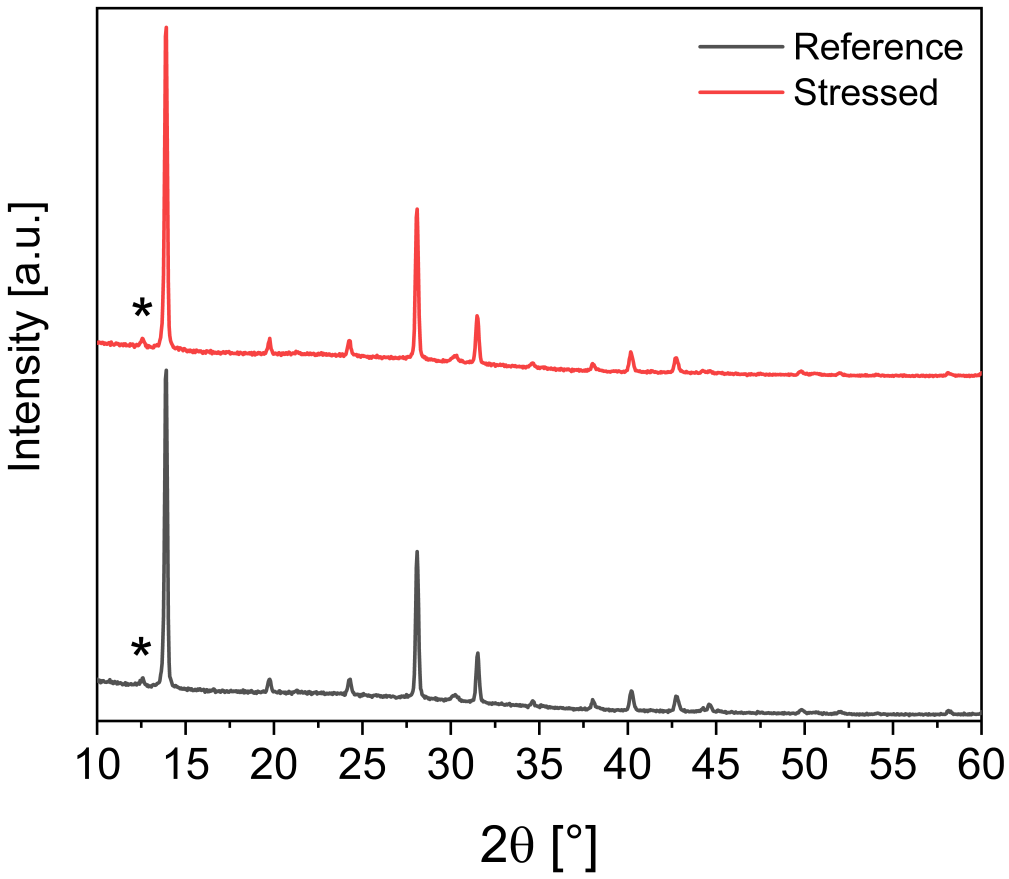

Figure 5: XRD patterns of a reference (grey) and PID stressed (red) device. The asterisk is indicating the peak around 12.5° representing the diffraction of the (001) plane of PbI_2.

objective of this ToF-SIMS analysis is to identify Na^+ migration into the perovskite absorber, the focus remains on the qualitative detection and distribution of Na^+. The different materials within the device are represented in distinct colors to aid in interpretation. The green line represents the Na^+ signal. A significant distinction is observed between the reference and stressed devices. In the reference device, Na^+ remains confined to the glass substrate, indicating no migration into the active layers. Conversely, the stressed device exhibits pronounced Na^+ diffusion throughout the entire structure, extending from the glass substrate to the C60/BCP electron transport layer.

4 Discussion

ToF-SIMS analyses, depicted in Figure 6, confirm the migration of Na^+ ions from the SLG substrate to the PSC under the influence of the electric field. This phenomenon is identified in the literature as the primary driver of the PID mechanism [17–20, 22]. The analyses revealed that Na^+ ions migrate through the entire stack of the PSC, reaching the ETL, beyond which the Na^+ signal intensity diminishes to negligible levels. Additionally, significant intensity peaks were observed at the interfaces near the NiO_X and LiF layers in the PID-stressed sample. However, it remains uncertain whether this effect is due to the accumulation of Na^+ ions or simply an artifact such as the matrix effect, which is frequently encountered in ToF-SIMS measurements [25, 26]. Further experiments incorporating advanced post-mortem microstructural analyses are required to clarify these observations and provide deeper insights into the underlying mechanisms. Notably, almost no Na^+ ions were detected in the reference device, except within the SLG.

These findings suggest that Na^+ drifts from the glass into the ITO of the stressed PSC under the

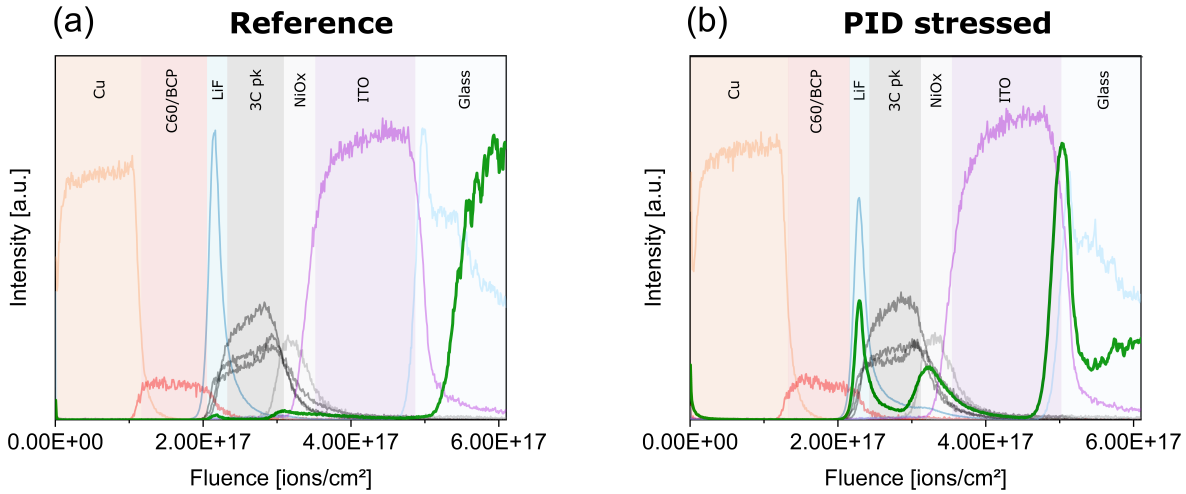

Figure 6: ToF-SIMS results of a reference (a) and PID stressed (b) PSC. The highlighted green line represents the data of the Na^+.

influence of the applied electric field, with degradation predominantly occurring during the first half of the PID test, corroborating previous research showing degradation with a negligible incubation period [23].

From the EQE response, a uniform decrease across the spectrum was noticeable, which suggests that the degradation affects the entire device rather than a specific interface. However, directly correlating EQE data to specific degradation locations within the device is challenging. Integration of the EQE responses and calculating relative differences with respect to the initial measurements reveals a relative decrease of 8%. The JV parameters indicated a normalized J_{SC} of 0.88, reflecting a 12% degradation from the initial measurements. Given that J_{SC} is derived from the integration of EQE data, similar values were anticipated from both measurements. Nevertheless, as noted by Saliba et al. [27, 28], a systematic discrepancy often exists between JV results and data obtained from EQE measurements. This known issue underscores the deviation in the J_{SC} values derived from IV and EQE measurements. Further experimental investigations are needed to elucidate the mechanisms underlying this discrepancy but are beyond the scope of this study [27, 28]. Nevertheless, EQE measurements using bias light can potentially lower the differences.

In addition to losses in J_{SC}, approximately 9% degradation in FF was observed, attributable to decreased shunt resistance and an increase in series resistance. Similar degradation effects have been documented in other studies [17–19, 22]. Literature suggests that the reduction in shunt resistance may be caused by a shunt pathway of Na^+ ions forming through the device, a phenomenon that has been visualized using 3D ToF-SIMS imaging techniques [17, 22]. Moreover, combined with the presented ToF-SIMS in Figure 6, it might be suggested that Na^+ is present at the device interfaces with the transport layers, potentially leading to an increase in series resistance, thus hindering carrier extraction.

In literature, Na^+ migration during PID stress has been shown to lead to perovskite segregation and decomposition [18, 19, 22]. It is stated that the migration of Na^+ forms weak bonds with the I from the perovskite, resulting in Na^+I^-. These effects have been confirmed through both XRD and PL measurements [18]. Specifically, PL data show a decrease in intensity combined with a redshift of the peak wavelength, indicating the presence of iodine-rich regions [18]. Additionally, XRD measurements reveal a decline in intensity around 14.5° suggesting perovskite degradation, along with the emergence of a peak around 12.5° confirming the presence of PbI_2 due to halide segregation [18].

However, when comparing these results from the literature with the findings of this study, several distinctions emerge. In this work, neither PL nor XRD analyses revealed significant differences between the stressed and reference devices. The PL measurements showed no observable differences in the wavelength at the peak position nor in the width of the peak. Therefore, one can suggest that the bandgap energy of the absorber material remained unchanged. Similarly, the XRD analyses revealed no differences between the stressed and reference devices; the peak around 14° remained stable, indicating no substantial changes in the perovskite material. Furthermore, the peak associated with PbI_2 around 12.5° remained unchanged,

implying no increase in PbI_2 content within the substrate. The presence of a small peak might stem from either precursor weighing or annealing of the substrate, but it is not considered a detrimental effect. Crucially, no significant differences were observed between the stressed and reference devices.

It is to be noted that this study was conducted using a stress setup that maximally eliminates unwanted additional degradation mechanisms [23]. Considering the less pronounced degradation patterns and the deviating PL and XRD results compared to the literature, it could be plausible that Na^+ migration induced by PID stress amplifies perovskite segregation and decomposition effects, potentially triggered by imperfections in device encapsulation. These imperfections may lead to exposure to undesired environmental degradation factors. Nevertheless, further research systematically incorporating additional environmental stressors is crucial to develop a comprehensive understanding of the observed phenomena. Moreover, it is noteworthy that the bandgap of the samples used in this research is lower than those reported in the literature [18, 19]. Perovskite materials with wider bandgaps are known to be more susceptible to halide segregation, likely due to their typically higher bromide (Br) content [29].

5 Conclusion

PID is recognized as a critical degradation pathway for perovskite devices, with literature documenting nearly complete performance loss within only 96 hours [16,18–22]. As a result, ensuring long-term stability is critical to advancing the commercialization of perovskite photovoltaics. A deeper understanding of PID's underlying physics is essential for developing targeted mitigation and prevention strategies.

Research on PID has largely identified Na^+ migration from SLG substrates to PSCs as a primary driver of degradation, often resulting in material segregation and decomposition. However, most of these studies have relied on encapsulated devices in ambient conditions, which may complicate the research into the effects of PID due to potential interactions with environmental stressors. Although PID stress methods that exclude other environmental stressors have been suggested in our previous work [23], their implementation requires dedicated equipment and controlled environments.

As a result, the aim of this study was to elaborate the effects of PID on perovskite devices in an inert environment using the suggested PID stress setup [23]. A relatively large batch of 48 p-i-n 3C PSCs was subjected to 313 hours of PID stress, with performance evaluated through intermediate and post-experiment measurements across a range of characterization techniques.

The findings demonstrated that PID is most aggressive in the initial half of the testing period (i.e., 150 hours), with a final normalized efficiency of 79%. ToF-SIMS analysis confirmed Na^+ migration throughout the device as presented in the literature [17, 22], with diminishing signal strength near the ETL interface, where peaks around other interfaces were also detected. Further investigation is required to determine whether these peaks indicate Na^+ accumulation at the interfaces or whether these peaks are mere artifacts, such as the matrix effect [25, 26].

Performance degradation was predominantly linked to reductions in J_{SC}, with moderate impacts on FF and negligible changes in V_{OC}, in line with results from prior work [23]. JV analysis revealed variations in both shunt and series resistance, suggesting the formation of a Na^+ shunt path within the device [17, 22], contributing to decreased shunt resistance. Moreover, the potential accumulation of Na^+ at the interfaces of the transport layers may impede carrier extraction, further impacting the device performance.

Interestingly, PL and XRD analyses revealed no signs of perovskite segregation or decomposition, diverging from previous studies [18,19,21,22]. This discrepancy challenges the conventional understanding of PID. It may suggest that environmental stressors such as moisture and oxygen could initiate degradation pathways, with Na^+ migration acting as an accelerant rather than the primary cause.

By employing a PID stress setup that eliminates external stressors, this study provides critical insights into the role of Na^+ migration in perovskite degradation. However, further microstructural characterization is necessary to elucidate its impact and develop effective mitigation strategies. Future studies should systematically introduce environmental stressors to resolve discrepancies with existing literature and clarify their potential interplay with PID. A deeper understanding of these complex ion interactions is essential for the development of durable and stable perovskite photovoltaic technologies.

6 Acknowledgements

The authors gratefully acknowledge the support of the "Fonds Wetenschappelijk Onderzoek" (FWO) and the FWO SB PhD fellowship under project number 1SD8323N. Special thanks are extended to Irene Dei Tos from Hasselt University for performing the XRD analysis and to Alexis Franquet from imec for conducting the ToF-SIMS measurements.

References

[1] B. A. Osman, T. M. Abdolkader, and I. S. Ahmed, "A review of perovskite solar cells," *International Journal of Materials Technology and Innovation*, vol. 1, pp. 48–66, 11 2021.

[2] R. A. Afre and D. Pugliese, "Perovskite solar cells: A review of the latest advances in materials, fabrication techniques, and stability enhancement strategies," *Micromachines 2024, Vol. 15, Page 192*, vol. 15, p. 192, 1 2024.

[3] S. Gholipour and M. Saliba, "Bandgap tuning and compositional exchange for lead halide perovskite materials," *Characterization Techniques for Perovskite Solar Cell Materials*, pp. 1–22, 1 2020.

[4] P. Chen, Y. Xiao, S. Li, X. Jia, D. Luo, W. Zhang, H. J. Snaith, Q. Gong, and R. Zhu, "The promise and challenges of inverted perovskite solar cells," *Chemical Reviews*, 10 2024.

[5] J. Y. Kim, J. W. Lee, H. S. Jung, H. Shin, and N. G. Park, "High-efficiency perovskite solar cells," *Chemical Reviews*, vol. 120, pp. 7867–7918, 8 2020.

[6] P. Zhu, C. Chen, J. Dai, Y. Zhang, R. Mao, S. Chen, J. Huang, and J. Zhu, "Toward the commercialization of perovskite solar modules," *Advanced Materials*, vol. 36, 4 2024.

[7] S. P. Feng, Y. Cheng, H. L. Yip, Y. Zhong, P. W. Fong, G. Li, A. Ng, C. Chen, L. A. Castriotta, F. Matteocci, L. Vesce, D. Saranin, A. D. Carlo, P. Wang, J. W. Ho, Y. Hou, F. Lin, A. G. Aberle, Z. Song, Y. Yan, X. Chen, Y. M. Yang, A. A. Syed, I. Ahmad, T. Leung, Y. Wang, J. Y. Lin, A. M. C. Ng, Y. Li, F. Ebadi, W. Tress, G. Richardson, C. Ge, H. Hu, M. Karimipour, F. Baumann, K. Tabah, C. Pereyra, S. R. Raga, H. Xie, M. Lira-Cantu, M. V. Khenkin, I. Visoly-Fisher, E. A. Katz, Y. Vaynzof, R. Vidal, G. Yu, H. Lin, S. Weng, S. Wang, and A. B. Djurišic, "Roadmap on commercialization of metal halide perovskite photovoltaics," *Journal of Physics: Materials*, vol. 6, p. 032501, 6 2023.

[8] L. Zhang, Y. Wang, X. Meng, J. Zhang, P. Wu, M. Wang, F. Cao, C. Chen, Z. Wang, F. Yang, X. Li, Y. Zou, X. Jin, Y. Jiang, H. Li, Y. Liu, T. Bu, B. Yan, Y. Li, J. Fang, L. Xiao, J. Yang, F. Huang, S. Liu, J. Yao, L. Liao, L. Li, F. Zhang, Y. Zhan, Y. Chen, Y. Mai, and L. Ding, "The issues on the commercialization of perovskite solar cells," *Materials Futures*, vol. 3, p. 022101, 4 2024.

[9] J. Huang, S. Tan, P. D. Lund, and H. Zhou, "Impact of h2o on organic–inorganic hybrid perovskite solar cells," *Energy & Environmental Science*, vol. 10, pp. 2284–2311, 11 2017.

[10] C. C. Boyd, R. Cheacharoen, T. Leijtens, and M. D. McGehee, "Understanding Degradation Mechanisms and Improving Stability of Perovskite Photovoltaics," *Chemical Reviews*, vol. 119, pp. 3418–3451, mar 2019.

[11] R. Wang, M. Mujahid, Y. Duan, Z. K. Wang, J. Xue, and Y. Yang, "A Review of Perovskites Solar Cell Stability," nov 2019.

[12] J. Li, R. Xia, W. Qi, X. Zhou, J. Cheng, Y. Chen, G. Hou, Y. Ding, Y. Li, Y. Zhao, and X. Zhang, "Encapsulation of perovskite solar cells for enhanced stability: Structures, materials and characterization," *Journal of Power Sources*, vol. 485, p. 229313, 2 2021.

[13] M. Cao, W. Ji, C. Chao, J. Li, F. Dai, and X. Fan, "Recent advances in uv-cured encapsulation for stable and durable perovskite solar cell devices," *Polymers 2023, Vol. 15, Page 3911*, vol. 15, p. 3911, 9 2023.

[14] W. Luo, Y. S. Khoo, P. Hacke, V. Naumann, D. Lausch, S. P. Harvey, J. P. Singh, J. Chai, Y. Wang, A. G. Aberle, and S. Ramakrishna, "Potential-induced degradation in photovoltaic modules: A critical review," 1 2017.

[15] H. Raza, T. Imran, Y. Gao, M. Azeem, M. Younis, J. Wang, S. Liu, Z. Yang, Z. Liu, and W. Chen, "Potential-induced degradation: a challenge in the commercialization of perovskite solar cells," *Energy Environ. Sci*, vol. 17, p. 1819, 2024.

[16] J. Carolus, T. Merckx, Z. Purohit, B. Tripathi, H. G. Boyen, T. Aernouts, W. De Ceuninck, B. Conings, and M. Daenen, "Potential-Induced Degradation and Recovery of Perovskite Solar Cells," *Solar RRL*, vol. 3, p. 1900226, oct 2019.

[17] K. Brecl, M. Jošt, M. Bokalič, J. Ekar, J. Kovač, and M. Topič, "Are Perovskite Solar Cell Potential-Induced Degradation Proof?," *Solar RRL*, p. 2100815, dec 2021.

[18] L. Nakka, W. Luo, A. G. Aberle, and F. Lin, "Study of Potential-Induced Degradation in Glass-Encapsulated Perovskite Solar Cells under Different Stress Conditions," *Solar RRL*, vol. 7, p. 2300100, jun 2023.

[19] L. Nakka, G. Shen, A. G. Aberle, and F. Lin, "Mitigation of Potential-Induced Degradation in Glass-Encapsulated Perovskite Solar Cells Using a NiOx Barrier Layer," *Solar RRL*, p. 2300582, sep 2023.

[20] L. Xu, J. Liu, W. Luo, N. Wehbe, A. Seitkhan, M. Babics, J. Kang, M. De Bastiani, E. Aydin, T. G. Allen, M. Alamer, W. Yan, F. Xu, A. U. Rehman, and S. De Wolf, "Potential-induced degradation in perovskite/silicon tandem photovoltaic modules," *Cell Reports Physical Science*, vol. 3, p. 101026, sep 2022.

[21] Z. Purohit, W. Song, J. Carolus, H. Chaliyawala, S. Lammar, T. Merckx, T. Aernouts, B. Tripathi, and M. Daenen, "Impact of Potential-Induced Degradation on Different Architecture-Based Perovskite Solar Cells," *Solar RRL*, vol. 5, p. 2100349, sep 2021.

[22] J. Zhang, H. Wu, Y. Zhang, F. Cao, Z. Qiu, M. Li, X. Lang, Y. Jiang, Y. Gou, X. Liu, A. M. Asiri, P. J. Dyson, M. K. Nazeeruddin, J. Ye, and C. Xiao, "Investigation of Potential-Induced Degradation and Recovery in Perovskite Minimodules," *Progress in Photovoltaics: Research and Applications*, sep 2024.

[23] R. Breugelmans, S. Lammar, A. Aguirre, T. Aernouts, B. Vermang, and M. Daenen, "Method to Study Potential-Induced Degradation of Perovskite Solar Cells and Modules in an Inert Environment," *Solar RRL*, vol. 8, jun 2024.

[24] R. Breugelmans, S. Lammar, A. Aguirre, T. Aernouts, B. Vermang, and M. Daenen, "Pet-based perovskite solar cells to avoid potential-induced degradation," *MRS Bulletin*, pp. 1–5, 12 2025.

[25] K. Takahashi, S. Aoyagi, and T. Kawashima, "Tof-sims matrix effects in mixed organic layers in ar cluster ion depth profiles," *Surface and Interface Analysis*, vol. 49, pp. 721–727, 8 2017.

[26] A. Priebe, T. Xie, G. Bürki, L. Pethö, and J. Michler, "The matrix effect in tof-sims analysis of two-element inorganic thin films," *Journal of Analytical Atomic Spectrometry*, vol. 35, pp. 1156–1166, 6 2020.

[27] M. Saliba and L. Etgar, "Current density mismatch in perovskite solar cells," *ACS Energy Letters*, vol. 5, pp. 2886–2888, 9 2020.

[28] M. Saliba, E. Unger, L. Etgar, J. Luo, and T. J. Jacobsson, "A systematic discrepancy between the short circuit current and the integrated quantum efficiency in perovskite solar cells," *Nature communications*, vol. 14, 12 2023.

[29] F. Penã-Camargo, P. Caprioglio, F. Zu, E. Gutierrez-Partida, C. M. Wolff, K. Brinkmann, S. Albrecht, T. Riedl, N. Koch, D. Neher, and M. Stolterfoht, "Halide Segregation versus Interfacial Recombination in Bromide-Rich Wide-Gap Perovskite Solar Cells," *ACS Energy Letters*, vol. 5, pp. 2728–2736, aug 2020.